Stabilization of half metallicity in Mn-doped silicon upon Ge alloying

S. Picozzi, F. Antoniella, A. Continenza, and A. MoscaConte
Istituto Nazionale di Fisica della Materia (INFM), Dipartimento Fisica Università L'Aquila, 67010 Coppito (Aq), Italy

A. Debernardi and M. Peressi
Istituto Nazionale di Fisica della Materia (INFM), Dipartimento Fisica Teorica, Università Trieste, I-34014 Grignano (Ts), Italy
(Received 7 January 2004; revised manuscript received 26 July 2004; published 18 October 2004)

We propose Si_xGe_{1-x} alloys as suitable candidates for spintronic applications. Remarkably, our first-principles investigation explains, within the local spin density approximation, the microscopic mechanism that stabilizes the half metallicity in Si matrices under Ge alloying and shows that it can spontaneously occur: in fact, half metallicity is determined by *p-d* hybridization in the presence of Ge atoms surrounding Mn impurities, and this particular environment is energetically favored over other possible local composition fluctuations, such as excess of Si atoms around Mn. A detailed discussion of the trends of defect formation energy and of magnetization as a function of alloy composition and configuration completes the present work.

DOI: 10.1103/PhysRevB.70.165205 PACS number(s): 75.50.Pp, 71.55.Cn

I. INTRODUCTION

Diluted magnetic semiconductors[1] (DMS's) represent one of the most recent, challenging, and exciting topics in the condensed matter area, due to the many unresolved issues from a fundamental point of view, as well as to the enormous potentialities as basic spintronic materials for device applications. So far, great interest has been devoted to transition-metal- (TM-) doped III-V semiconductors [having its prototype in MnGaAs (Refs. 2–4)] and to TM-doped oxides [the prototype being $Co_xTi_{1-x}O_2$ (Ref. 5)]. Recently, however, some attention[6–11] has been devoted to TM-doped group-IV semiconductors (in particular to Mn-, Cr-, and Fe-doped Ge): in this case, the complexity related to the chemical environment with the consequent presence of defects (such as As_{Ga} antisites in MnGaAs) is believed to be reduced thanks to the single atomic species of the host matrix. This might open the way to a better understanding of the fundamental mechanisms leading to the observed ferromagnetism (FM). Heteroepitaxial growth of Mn_xGe_{1-x} thin films has been achieved and reported by a few groups[6,7] and showed Curie temperatures up to 116 K, along with a *p*-type character and hole-mediated exchange.[6] Higher Curie temperatures (up to 285 K) were also reported for Mn-doped bulk Ge single crystals.[8] From the theoretical point of view, several density-functional-based studies were undertaken. In particular, a Ruderman-Kittel-Kasuya-Yoshida (RKKY) mechanism was invoked to explain the exchange interactions in Mn_xGe_{1-x} as a function of the Mn local environment.[12] Accurate full-potential linearized augmented-plane-wave[13] (FLAPW) calculations were performed by some of us[14] for $Mn_x(IV)_{1-x}$ (IV = Si, Ge) systems, suggesting Mn to be a source of holes and localized magnetic moments of about $3\mu_B$/Mn. Moreover, ferromagnetic alignment was found to be favored over antiferromagnetism, its stabilization generally increasing with Mn content. Irrespective of the Mn content, Ge-based systems were found to be very close to half metallicity, whereas the Si-based structures just missed the half-metallic behavior due to the crossing of the Fermi level by the lowest conduction bands. Very recently, the energetics of interstitial and substitutional Mn in Si, Ge, and Si_xGe_{1-x} alloys has been investigated by means of first-principles calculations;[15] for $x \leqslant 0.84$, substitutional Mn in a Ge-rich neighborhood was found to be more stable than interstitial Mn.

A combined theoretical and experimental study was focused on Cr_yGe_{1-y} and $Cr_yMn_xGe_{1-x-y}$(001) thin films grown on GaAs(001) (Ref. 11) the samples were found to be strongly *p* type, with the hole density increasing with Cr concentration. Cr_yGe_{1-y} systems were paramagnetic for the growth conditions and low Cr concentrations employed ($y < 0.04$), in agreement with first-principles predictions. Addition of Cr into the ferromagnetic semiconductor Mn_xGe_{1-x} host, however, systematically reduced the Curie temperature and the total magnetization.

An interesting question to address is whether the occurrence of half-metallicity found in some of the Mn:Ge systems results from long-range effects or rather from short-range interactions. In the former case, it would be interesting to know the critical composition *x* which would cause the loss of half-metallicity in Mn-doped Si_xGe_{1-x} alloys, while, in the latter case, it would be desirable to understand how the local environment—from both chemical and structural points of view—affects half metallicity. In this work, we extend the previous study reported in Ref. 14 and focus on the effect of the Si-Ge relative composition. SiGe alloys have been the object of several theoretical as well as experimental investigations[16] due to their technological relevance in the realization of multiple-well and quantum-dot systems. Moreover, strain effects in these systems have been deeply investigated and exploited in the design of new devices. Due to the importance of Si in modern technology, the possibility of Mn doping in suitable Si:Ge-diluted systems, properly tailored to adjust matching constraints, might open the way to realize the integration of magnetic semiconductors into Si-based devices. Moreover, these systems offer a base of investigation to ascertain the effects of the chemical and structural environment on the ferromagnetic properties.

In this study, we concentrate on the electronic and magnetic properties of Mn impurities in Si_xGe_{1-x} alloys at differ-

TABLE I. Atomic shells $S_i (i=1,\ldots,5)$ in a 32-atom bcc supercell and their filling according to the Si_xGe_{1-x} alloy composition x for the different studied systems as a function of concentration x in Si_xGe_{1-x} host matrices. In parentheses, we show the number of independent sites of each shell. In all the systems considered, the Mn atom is located at the origin.

x	S_1 (1)	S_2 (4)	S_3 (12)	S_4 (12)	S_5 (3)
0.0	Mn	Ge	Ge	Ge	Ge
0.094	Mn	Ge	Ge	Ge	Si
0.125	Mn	Si	Ge	Ge	Ge
0.25	Mn	Si	Ge	Ge	Si
0.375 R_1	Mn	Ge	Si	Ge	Ge
0.375 R_2	Mn	Ge	Ge	Si	Ge
0.5 R_3	Mn	Si	Ge	Si	Ge
0.5 R_4	Mn	Ge	Si	Si	Ge
0.75	Mn	Ge	Si	Si	Si
1.0	Mn	Si	Si	Si	Si

ent x concentrations. Due to the limited solubility of Mn in group-IV semiconductors, we limit our study to small Mn concentrations and describe the impurity limit using supercells with one substitutional Mn impurity only. As already pointed out,[15] substitutional Mn is generally favored over the interstitial site, whereas, for large Si concentrations in the Si_xGe_{1-x} host, interstitial Mn is expected to be favored. However, in order to focus on trends of relevant structural, electronic, and magnetic properties as a function of the x concentration, we limit our study to the substitutional Mn site.

In Sec. II we report computational and structural details; in Sec. III we discuss our results, in terms of energetics, structural, electronic, and magnetic properties as a function of the relative concentration x in Mn-doped Si_xGe_{1-x} alloys, both using the "real-atom" (RA) and "virtual-crystal" (VC) approaches. Finally, we summarize our results and draw the conclusions.

II. TECHNICALITIES

A. Computational details

The calculations in this work were performed using the PWSCF package[17] within the local spin density approximation (LSDA) to density functional theory. As is well known, this scheme does not allow an exact evaluation of the exchange-correlation interactions, which may affect the electronic and magnetic properties of these correlated compounds. In particular, the effects on the unoccupied states might be relevant, as shown in Refs. 18 and 19 by means of LSDA + self-interaction-correction (LSDA+SIC) and LSDA+U calculations, respectively, for the similar GaMnAs compound. An ultrasoft (US) pseudopotential[20] (PP) was used for Mn, with semicore 3*p* and 3*s* states kept in the valence shell while Si and Ge were described using a norm-conserving PP. The kinetic energy cutoff used for the wave functions was fixed at 25 Ry; a 250 Ry cutoff was chosen for the charge density, due to the presence of the US Mn pseudopotential. The irreducible wedge of the zinc-blende Brillouin zone was sampled with a (444) Monkhorst-Pack[21] mesh. Si_xGe_{1-x} alloys $(0<x<1)$ were simulated in two ways: (1) by means of the virtual-crystal approximation, in the Ramer-Rappe[22] implementation, using pseudopotentials in separable form;[23] this allows formulation of the virtual-ion PP in terms of the Kleinman-Bylander projectors of the true pseudopotentials and a simple mixing of the local potential contributions; and (2) using real atoms to investigate the role of the local environment.

In order to evaluate the numerical uncertainty, we compare our pseudopotential calculations with those obtained with the FLAPW method for some selected Mn-based structures such as bulk bcc Mn, [001]-ordered antiferromagnetic (AFM) Mn, ideal MnSi and MnGe zinc-blende compounds, and diluted Mn_xSi_{1-x} alloys. Taking into account also the numerical uncertainty in pseudopotential calculations due to convergence parameters, we found that estimated errors were of (i) less than 0.1 eV on the *relative* formation energies, (ii) about 0.01 Å on the bond lengths, and (iii) about $0.05\mu_B$ on the magnetic moments. As shown in the following, none of these numerical errors is going to affect the physical picture that emerges from the results.

B. Structural details

In order to simulate random semiconducting alloys from first principles, several approaches have been proposed.[24–26] Here, for the Si_xGe_{1-x} alloy $(0\leqslant x\leqslant 1)$, which is the matrix for the substitutional Mn impurity, we adopted the approach proposed by Baldereschi and Peressi[27] for both ionic and semiconducting solid solutions, based on cubic supercells, filled shell by shell with Ge and Si atoms according to cubic symmetry. This symmetry constraint limits the allowed compositions and the internal distortions that can be described by a given supercell. In particular, we used here a 32-atom bcc cell, its Bravais vectors being $a_1=(a_0,a_0,a_0)$, $a_2=(-a_0,a_0,a_0)$, and $a_3=(-a_0,-a_0,a_0)$, where a_0 is the cubic lattice constant of the host compound. The atomic shells (denoted $S1$, $S2$, $S3$, $S4$, and $S5$ in Table I) contain, respectively, 1, 4, 12, 12, and 3 atoms (see Table I) and therefore allow for composition $x=0.03125$, 0.09375, 0.125, 0.15625,

TABLE II. Relevant properties of a Mn impurity in a Si_xGe_{1-x} matrix as a function of the Si concentration, x: lattice constant (a in a.u.), difference of defect formation energy (ΔH_f, in eV) with respect to the Mn-doped Ge system taken as reference, total (μ_{tot}) and absolute (μ_{abs}) magnetization (both in Bohr magnetons), Mn nearest-neighbor distance and ideal nearest-neighbor distance (d(Mn-NN), d(NN), respectively, in a.u.).

					0.375		0.5			
x	0.0	0.094	0.125	0.25	R_1	R_2	R_3	R_4	0.75	1.0
a	10.650	10.611	10.597	10.545	10.492	10.492	10.440	10.440	10.335	10.230
ΔH_f	0.00	0.00	0.15	0.17	0.09	0.04	0.25	0.09	0.15	0.33
μ_{tot}	3.03	3.01	2.91	2.96	3.00	2.97	2.77	3.00	2.97	2.73
μ_{abs}	4.06	4.03	3.81	3.80	4.07	3.90	3.59	4.02	3.95	3.59
d(Mn-NN)	4.55	4.54	4.47	4.48	4.55	4.51	4.44	4.53	4.51	4.43
d(NN)	4.61	4.59	4.59	4.57	4.54	4.54	4.52	4.52	4.48	4.43

0.21875, 0.25, 0.375, 0.40625, 0.46875, and 0.5 of the undoped Si_xGe_{1-x} alloy and for the complementary ones.

In the systems considered, we fully relaxed all the internal positions according to the *ab initio*—calculated atomic forces; therefore, local strain effects are correctly taken into account. For the pure end points (i.e., $x=0$ or $=1$), the calculated bulk lattice constants were $a_0^{Si}=10.23$ a.u. and $a_0^{Ge}=10.65$ a.u., in good agreement with the corresponding experimental values ($a_0^{Si}=10.26$ a.u. and $a_0^{Ge}=10.69$ a.u.). As for $0<x<1$, the average lattice constant has been calculated according to Vegard's law—i.e., by means of a linear interpolation between the end points. This is justified by already published[16,28] results and confirmed by some of our tests.

We note that undoped Si-Ge isotropic cells reproduce satisfactorily the main experimental trends as far as individual bond lengths ($d_{i\text{-}j}$ with i, j=Si, Ge) are concerned; we find that the relevant bond lengths show quite small variations as a function of the concentration: $d_{Ge\text{-}Ge}$ varies between 4.58 and 4.61 a.u., $d_{Si\text{-}Ge}$ between 4.52 and 4.54 a.u., and $d_{Si\text{-}Si}$ between 4.46 and 4.50 a.u. which compare very well with the experimental[29] and previous theoretical[16,28] values (4.61, 4.53, and 4.44 a.u., respectively, with error bars of about 0.02 a.u.). Of course, the structures considered are only a very simple possible choice to represent a complex system such as the Si_xGe_{1-x} alloy: much larger cells along with different site occupation criteria should be considered for a better description of the randomness effects. However, our findings give us confidence that the present simple model is sufficient to obtain the main important results for the undoped alloy in terms of formation energies and structural and electronic properties, and it can be easily extended to the case of Mn doping in order to describe reliably the effects of different local environments around the impurity on the macroscopic quantities listed above. Moreover, as we will show in detail, the overall magnetic properties of the compound are essentially determined by the *local* environment, so that our simple structures can already be representative of some of the possible occurring cases.

In the case of Mn doping, we extend this simple model considering the Mn impurity at the center of the cell and using the isotropic filling criterium for the remaining atomic shells. This allows for almost the same alloy compositions listed for the undoped alloy. Here, we explicitly consider the compositions $x=0$, 0.09375, 0.125, 0.25, 0.375, 0.5, 0.75, and 1. In Table I we report the chemical occupation of the different atomic shells for different selected composition x of the Si_xGe_{1-x} host matrices. For each composition, the lattice constant is taken equal to that of the undoped case; again, our tests show that this is a good approximation, due to the very small Mn concentration.

III. Mn DEFECTS IN A Si_xGe_{1-x} MATRIX

In this section, we will discuss the results for a single Mn impurity as a function of the different host matrix—i.e., by (i) varying the Si concentration x in the Si_xGe_{1-x} matrix and (ii) comparing the VC and the corresponding structures with *real* atoms at the same concentration value x. In Table II we show the relevant properties of the different systems, in terms of formation energy (H_f) differences, structural parameters [lattice constants and Mn nearest-neighbor (NN) bond lengths], and total (μ_{tot}) and absolute (μ_{abs}) magnetization, which are defined as $\mu_{tot}=\int d\mathbf{r}[\rho_\uparrow(\mathbf{r})-\rho_\downarrow(\mathbf{r})]$ and $\mu_{abs}=\int d\mathbf{r}|\rho_\uparrow(\mathbf{r})-\rho_\downarrow(\mathbf{r})|$, respectively.

We remark that, in the following, we will discuss results obtained using the local spin density approximation; of course, a different treatment of exchange and correlation effects might change some of the conclusions, in particular those related to the half-metallic versus metallic character of the different systems.

A. Formation energies

Let us first consider the real-atom case. The formation energy for a Mn impurity in a Si_xGe_{1-x} matrix is evaluated as $H_f=E^{def}-E^{pure}-\mu^{Mn}+\mu^{IV}$, where E^{def} and E^{pure} are the total energies of the unit cell with and without Mn defect—which substitutes for the group-IV atom—respectively; μ^{Mn} (μ^{IV}) is the chemical potential of a bulk Mn (group IV). As a reference for the Mn chemical potential, we considered the value in the AFM [001]-ordered fcc lattice. Only neutral defects are considered. Of course, both the assumptions of neglecting (i) Mn_xGe_y or Mn_xSi_y competing phases in the Mn chemical potential and (ii) charged states are arbitrary choices which may affect the final results.[30]

We found that the formation energy is very sensitive to the kinetic energy cutoff employed for the plane-wave expansion set; with the cutoff used here, we estimate an *absolute* numerical uncertainty of about 0.5 eV. We find quite large values ($>$1.5 eV, clearly beyond our numerical uncertainty) for the formation energies of all the systems considered, which highlights the difficulties in doping Si_xGe_{1-x} alloys with Mn; this is consistent with the experimentally observed[6] tendency towards clustering of Mn atoms and/or formation of different magnetic phases (such as $Mn_{11}Ge_8$) at Mn concentrations higher than about 10%.

We point out that, despite the quite large numerical uncertainty in the H_f *absolute* value, its *relative* variations with respect to the host chemical composition are much less sensitive to computational details (the *relative* numerical uncertainty being less than 0.1 eV). A comparative analysis of the formation energies for the different compositions and configurations is therefore possible and meaningful. We choose as reference system a Mn impurity in a Ge host, where H_f reaches its minimum, and we report in Table II the differences of the formation energies with respect to that case. Usually, the formation energy and magnetization are considered to be a function of one parameter only: the concentration x. Looking at the results displayed in Fig. 1, we notice that this statement can be valid only to a first, quite rough, approximation. The estimate of ΔH_f based on the end points (pure Si or Ge matrix) only may suggest that the formation energy regularly increases with Si concentration. However, even from a first look at the results reported in Table II and in the first panel of Fig. 1 (open symbols), we find that the *average composition* is not the only important quantity. In fact, at a given composition, sizable fluctuations of ΔH_f occur for different specific *configurations*. This is related to the relevance of the local environment (i.e., limited to the NN shell): in the case of a Si NN shell, we find formation energies larger than those corresponding to systems where Mn is surrounded by a Ge NN shell, thus evidentiating the lower energy cost of Mn to bind with Ge rather than Si. This is consistent with the results of da Silva *et al.*,[15] who varied the number of Si versus Ge neighbors in the Mn first coordination shell (denoted as ν) and found that Ge-rich neighboorhoods have lower formation energies [i.e., the formation energy decreases about 0.3 eV in going from $\nu=0$ (i.e., no Si as nearest neighbor) to $\nu=4$ (i.e., no Ge as nearest neighbor)].

Moreover, the two structures R_1 and R_2 with equal concentration at $x=0.375$ have different formation energies and different magnetizations, as a consequence of the fact that they correspond to filling of shells at different distances from the Mn impurity. As expected, single shells contribute differently, according to the distance from the Mn atom. This is particularly evident for the formation energy.

We did not investigate all the complementary configurations; however, we payed much attention to low Si concentration—which is also the most favored case—and study the behavior of the formation energy upon filling up with silicon atoms only one shell at a time—namely, only $S2$, $S3$, $S4$, or $S5$. Considering these structures (namely, $x=0.125$, $R1$, $R2$, and $x=0.094$, in Tables I and II) and comparing their formation energy with those corresponding to the other structures of Table I we notice that (i) the contribution to ΔH_f per Si atom decreases as the order of the shell increases, going from 0.04 eV of the nearest-neighbor shell to 0.007, 0.003, and 0.000 eV for the second-, third-, and fourth-neighbor shells, respectively, showing an almost exponential trend; (ii) the contributions to ΔH_f per Si atom of each of the four neighbor shells considered are almost additive. In fact, summing the contributions of the various shells we obtain 0.28 eV, in substantial agreement with the value of 0.33 eV found for the direct calculation of Mn impurity in pure Si. Similar considerations also hold for the other structures of Table I. The additivity of the single-shell contributions denotes a relatively small three-body contribution with respect to the relevant two-body Mn-Si (or Mn-Ge) direct interaction.

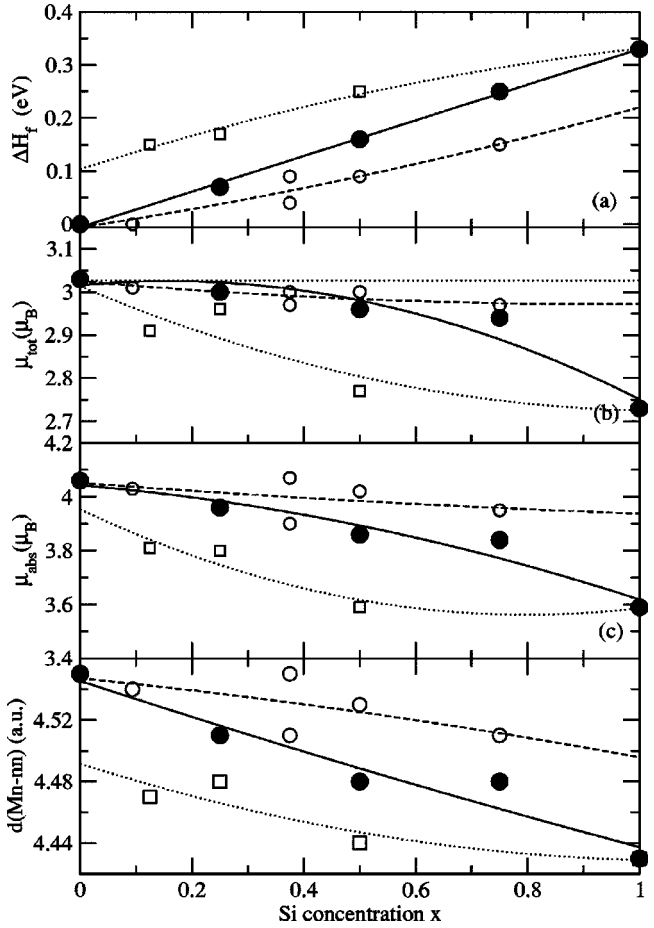

FIG. 1. (a) Formation energy difference (ΔH_f), (b) total magnetic moment (μ_{tot}), and (c) absolute magnetic moments (μ_{abs}) as a function of concentration x in Mn-doped Si_xGe_{1-x} alloys for VC systems (solid circles). For comparison, values for the RA systems are also shown (open symbols): squares if NN of Mn are Si, circles if they are Ge. Dotted and dashed lines are a guide to the eye connecting configurations with similar local environments.

For completeness, we also discuss the results for the VC case; by its nature, the VC model accounts for the average composition only and neglects details of the local environment. In general, the results from the VC model (solid symbols in Fig. 1) show regular trends of the different properties

TABLE III. Total and absolute magnetic moments (in μ_B) of the Mn impurity in pure Ge and Si matrices at different lattice constants (see text).

		$a=10.230$ a.u.	$a=10.440$ a.u.	$a=10.650$ a.u.
Mn in Ge	μ_{tot}	2.92	3.00	3.03
	μ_{abs}	3.73	3.98	4.06
Mn in Si	μ_{tot}	2.73	2.95	2.98
	μ_{abs}	3.59	3.91	4.00

with the average composition of the host alloy. As for ΔH_f, in particular, the dependence on x is almost linear, and this behavior is also recovered by averaging the different values for the different possible configurations with real atoms.

B. Structural properties

The study of hypothetical MnGe and MnSi zinc-blende compounds shows a sizable reduction of the lattice parameter with respect to the corresponding pure Si and Ge bulks: the equilibrium bond lengths as calculated within PWSCF-LSDA are found 4.48 a.u. and 4.32 a.u. for MnGe and MnSi, respectively—i.e., 0.13 a.u. and 0.11 a.u. less than those of the corresponding group-IV elements. This suggests that sizable local lattice contractions must join the substitution of Mn impurities into Si_xGe_{1-x} alloys. This is indeed found from the analysis of the individual Mn NN distances in the different configurations, together with other opposite relaxations for nontrivial compensation effects taking into account the average matrix composition. If the NN's of Mn are Ge, the $d_{Mn\text{-}Ge}$ distances are always smaller than d_{NN}(Ge) in bulk Ge, but remain larger than d_{NN}(MnGe) in the MnGe zinc blende. At variance, if the NN's of Mn are Si, the $d_{Mn\text{-}Si}$ distances are always equal or larger than d_{NN}(Si) in bulk Si. As a common feature, the $d_{Mn\text{-}NN}$ bond lengths are in between the d_{NN}(Ge) and d_{NN}(Si) in the corresponding elemental bulk.

This suggests that both chemical (related to the dominant hybridization in DMS's, between Mn *d* states and anion Si vs Ge *p* states) and size (related to the Si vs Ge local environment) effects are quite important in determining the final local structure and the consequent stability.

C. Magnetic properties

Similar considerations hold to explain the magnetization trends: a total magnetic moment very close to $3\mu_B$—presumably leading to half-metallicity; see below—is found in systems where the TM impurity is bonded with Ge atoms, whereas, in the case of a Mn-Si bond, the magnetic moment is reduced to about $(2.7-2.8)\mu_B$, leading to a situation where half metallicity is just missed.

However, as is well known, magnetic properties are very often strongly dependent on the volume and this is also true in these compounds. In order to separate chemical from volume contributions, we show in Table III the total and absolute magnetic moments for $x=0$, 1 at different volumes. The structure MnGe (MnSi) at $a=a_{Si}$ ($a=a_{Ge}$) is obtained from the fully relaxed MnSi (MnGe) at $a=a_{Si}$ ($a=a_{Ge}$) by a simple exchange of group-IV atoms; those at the $Si_{0.5}Ge_{0.5}$ lattice constant are at the ideal unrelaxed zinc-blende posistions. The general trend of larger magnetic moments at larger volumes is confirmed in both compounds; however, we can observe that, at fixed volume, Mn in Ge always shows a larger magnetization than Mn in Si. Moreover, we can see that the total magnetic moment of Mn in Si at intermediate lattice constant ($a=a_{Si_{0.5}Ge_{0.5}}=10$ a.u.) is appreciably larger ($2.95\mu_B$) than in the R_3 structure ($2.77\mu_B$; cf. Table II), where Mn is also surrounded by Si atoms and where the average lattice constant is the same. This is a mere local strain effect, due to the full relaxations allowed in the alloy case (R_3 structure) that lead to a Mn-Si distance ($d_{Mn\text{-}NN}=4.44$ a.u.) much shorter than in the ideal case (4.52 a.u.). In this situation, therefore, local strain relaxation dictated by the Si size strongly suppresses the magnetic moment.

The apparently anomalous case of $Si_{0.25}Ge_{0.75}$, where the magnetic moment is close to three, despite Si being the Mn NN, can be explained on the basis of the same arguments: here the larger Mn-Si distance, combined with the larger lattice constant, results in an enhanced total magnetic moment, close to Mn in pure Si at the average Ge-Si lattice constant.

The reason for this behavior can be traced back to the *p-d* hybridization and related exchange splitting (see below). However, as a general trend, we can conclude that the resulting magnetic moment is determined by the interplay of size and chemical effects related only to the NN shell or, equivalently, that the local environment around the Mn impurity is the main ingredient in determining the final electronic and magnetic properties. The higher value of the absolute magnetization, compared to the total magnetization, denotes the presence of antiferromagnetic regions; this is well known,[14] since the polarization induced on the NN shell is generally negative. This is also confirmed by the present results: for example, calculations of the Löwdin charges[31] in the $x=0.5$ case show that the polarization induced on the NN Ge and Si atoms is $-0.13\mu_B$ and $-0.12\mu_B$ in the R_4 and R_3 cases, respectively. Also for the absolute magnetization, similar arguments—in terms of chemical and size effects of the local environment—can be invoked to explain the trends as a function of the Si_xGe_{1-x} concentration x.

In this regard, it is interesting to study how the induced spin polarization behaves as the distance from the Mn impurity is increased. In Fig. 2 we show the magnetic moment on atomic positions belonging to successive neighbor shells, calculated as the difference of the Löwdin charges for up- and down-spin states: the curves plotted in Fig. 2 differ only for the magnetic moment value on the Mn impurity (located at the cell origin); as the distance from the magnetic impurity is increased, the induced spin polarization is the same, irrespectively of the chemical species occupying the *n*th neighboring shell. This shows that we are dealing with a mere local effect, which is very little affected by the *average* composition and *long-range* ordering of the host matrix.

If we look at the results of the VC calculation in Fig. 1, we find that, since local effects are wiped out, the behavior is

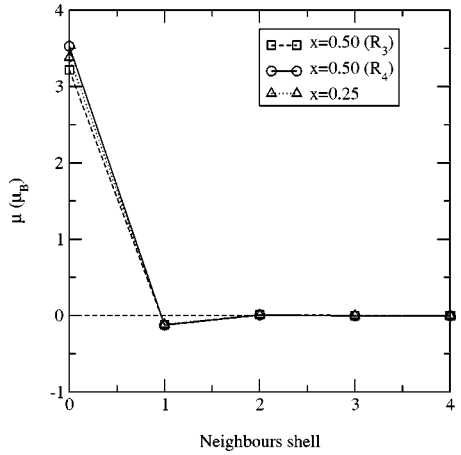

FIG. 2. Magnetic moment μ (μ_B) on the atomic sites occupying different neighboring shells as a function of the distance from the Mn impurity placed at the origin of the cell. The different curves are relative to different Si_xGe_{1-} x concentrations.

more regular and less scattered than in the RA case: here, both μ_{tot} and μ_{abs} show a deviation from the linear trend; in particular, for both total and absolute moments, a parabolic fit (i.e., a linear trend plus a quadratic term related to the bowing) is a reasonable approximation, the deviation being comparable to our estimated numerical uncertainty.

D. Electronic properties

In order to deeper investigate the electronic and magnetic properties, we focus on the 50% case and report in Fig. 3 the total density of states (DOS), along with the DOS projected (PDOS) on the Mn impurity and on the first NN Si or Ge for both R_3 and R_4 cases. As expected, a strong hybridization is found between the Mn d and group-IV p states, along with a Mn atom showing a minority DOS mostly unoccupied [cf. Fig. 3, panels (c) and (d)]; this feature is common to most DMS's. From the total DOS, it is clear that the two systems, though showing similar features, remarkably differ for the position of the Fermi level, E_F, with respect to the conduction bands, the R_4 (R_3) system showing (not showing) half metallicity. In particular, the density of states for the majority-spin bands are almost exactly equal; on the other hand, for the minority-spin component, the occupied states still show a very similar behavior, whereas the unoccupied bands are systematically lower (by as much as 0.2 eV) in the R_3 case compared to the R_4 case, due to the lower-energy position of the Mn $e_g^{\downarrow}$ bands [see the peak at about 0.3–0.5 eV in Figs. 3(c) and 3(d)]. This can be traced back to the exchange splitting, which, due to the larger Mn $d-$(IV)p hybridization, is smaller in the case of the Mn-Si bond (present in R_3) compared to the Mn-Ge bond (present in R_4).

In Fig. 4 we plot the density of states projected on the Mn site and resolved in t_{2g}- and e_g-like symmetry for the Si_xGe_{1-x} alloy at $x=0.25$ and $x=1.0$, panels (a) and (b), respectively. The case of the Mn impurity into a Si matrix

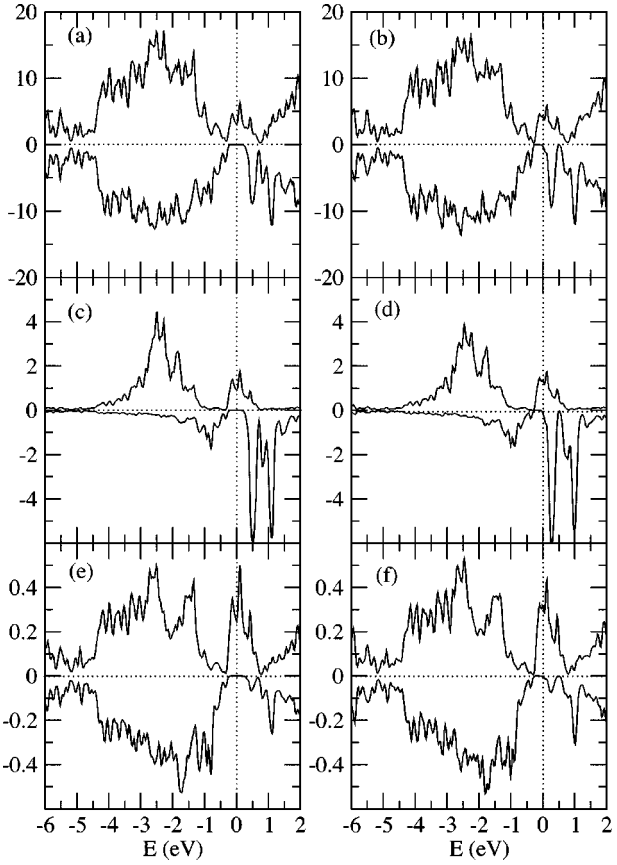

FIG. 3. Density of states for the $x=0.5$ concentration: (a), (b) Total density of states for R_4 and R_3 systems, respectively. Density of states projected on (c) Mn in R_4, (d) Mn in R_3, (e) Ge NN in R_4, and (f) Si NN in R_3. Positive and negative values are relative to the majority- and minority-spin states, respectively.

[panel (b)] is quite close to the case of Mn in GaAs (Ref. 32): we find majority bonding t_{2g}-like states at higher binding energy and with spatial localization on the Mn, completely filled. The Fermi level cuts at almost half-filling the t_{2g}-like antibonding majority states with spatial localization on the Si site and touches the minority e_g-like states poorly hybridized with Si states. Comparing Fig. 3 for the 50% SiGe alloys (R_3 and R_4) with Fig. 4 [panel (b)] for the Mn impurity in pure Si, we can see that the projected DOS on the Mn sites are very similar: the minority states with e_g symmetry are located at the same energy position above the Fermi level and are slightly occupied, causing the loss of half-metallicity. We remark, however, that the Fermi level position with respect to the highly localized e_g states is strongly dependent on the treatment of the exchange-correlation interaction. Preliminary LSDA+U calculations where U is self-consistently determined[33] suggest that $U\approx 3.0$ eV is appropriate for Mn in Si and Ge environments. For this value of U, half-metallic behavior is recovered in Mn-doped Si as well. Other relevant results discussed here, such as the formation energy trends, are unchanged within LSDA+U. We caution the reader that previous LSDA+U calculations used to fit photoemission spectroscopy data for substitutional Mn inpurities in other

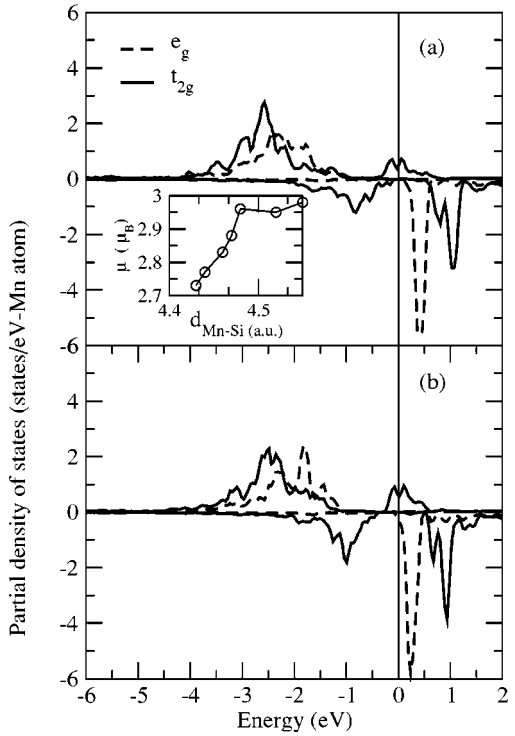

FIG. 4. Projected density of states on the Mn site resolved into states with t_{2g}- and e_g-like symmetries for the Si_xGe_{1-x} alloy with $x=0.25$ and $x=1.0$ [panels (a) and (b), respectively]. The inset shows the total magnetic moment behavior as a function of the Mn-Si distance in structures having Mn surrounded by four Si atoms.

semiconductors (III-V and II-VI) indicate values of U varying from 2 eV (Ref. 32) to 4 eV (Ref. 34) with a rather large uncertainty (1 eV according to Ref. 35). Therefore our finding based on preliminary LSDA+U calculations awaits both for experimental validations and deeper theoretical investigation. In general, the effect of the exchange-correlation treatment as a function of the different SiGe composition on the electronic and magnetic properties of these compounds needs to be carefully investigated and is beyond the goals of the present work.

The PDOS for the Si_xGe_{1-x} at $x=0.25$ [Fig. 4, panel (a)] shows the minority e_g-like states at energies higher than the Fermi level and completely empty, leading to an higher total magnetic moment and to a character very close to half-metallic. Now, going back to Table II, we can see that the main difference among the $x=0.25$, 0.5, and 1.0 alloys (all having Si as first coordination shell of Mn) is the $d_{Mn\text{-}NN}$ distance: very similar in the $x=0.5$ and 1.0 cases and smaller than at $x=0.25$ concentration. A smaller $d_{Mn\text{-}NN}$ distance increases the hybridization of the Mn d states with the Si p states, thus reducing the e_g exchange interaction: this is a crucial mechanism in the bond-length range we are exploring, as clear from the inset of Fig. 4 showing the total magnetic moment behavior as a function of the $d_{Mn\text{-}NN}$ distance. As we can see, the magnetic moment is very sensitive to the local distances: the minority e_g states being very well localized in energy, a small change in their energy position causes dramatic effects in terms of occupation of minority states and total magnetic moment.

The situation for Ge is rather different: the exchange splitting being larger than in Si, as shown in Fig. 3, the e_g-like minority states are empty and well above the Fermi level, in the bond-length range of interest; therefore, structures with Ge in the nearest coordination shell of the Mn impurity always show a stable and quite large total magnetic moment, consistent with a character very close to half metallicity.

In summary, our calculations for Mn-doped Si_xGe_{1-x} alloys show that, for a given concentration x, the local environment can dramatically change the electronic and magnetic properties and, in particular, the conducting character (i.e., metallic versus half-metallic) of the system. In particular, within LSDA, when Mn has Si as first NN, the Mn-Si hybridization reduces the exchange splitting, so that E_F is shifted from the minority band gap towards the lowest conduction bands, rendering the system less appealing for spintronic applications. On the other hand, a Ge NN shell around the Mn defect is favored from the energetic point of view and results in half metallicity, therefore opening the way to group-IV-based spintronic devices.

IV. CONCLUSIONS

Accurate first-principles pseudopotential calculations within the local spin density approximation to the density functional theory have been performed for Si_xGe_{1-x} alloys doped with Mn, focusing on the structural, electronic, and magnetic properties as a function of the host matrix and distribution of Mn atoms.

We have shown that Si_xGe_{1-x} alloys are suitable candidates for spintronic applications. The presence of Si guarantees the desired integrability with the well-assessed Si technology, whereas the presence of Ge stabilizes the desidered magnetic properties. In fact, our results show that half metallicity, typical of some diluted magnetic semiconductors, is very sensitive to the exchange-correlation treatment and to the local environment around the Mn impurity: within the LSDA, for those systems where Mn is surrounded by Ge atoms, half metallicity is preserved for all the considered x range, whereas it is generally lost when Si atoms are first nearest neighbors of the Mn impurity. This has been explained in terms of p-d hybridization, which affects the exchange splitting and results in a Fermi level that can move from the minority band gap up within the conduction band, therefore changing the character from half-metallic to metallic. Remarkably, the calculated formation energies show that a local Ge environment around Mn impurity is favored over a Si local environment: therefore, these systems, along with the desired half metallicity, hold promise for spintronics applications.[35]

ACKNOWLEDGMENTS

We gratefully acknowledge support from INFM through Iniziativa Trasversale Calcolo Parallelo. Work in L'Aquila supported by INFM through PAIS-GEMASE.

[1] H. Ohno, Science **281**, 951 (1998); T. Dietl, H. Ohno, F. Matsukura, J. Cibert, and D. Ferrand, *ibid.* **287**, 1019 (2000).
[2] S. Sanvito, G. Thuerich, and N. A. Hill, J. Supercond. **15**, 85 (2002).
[3] J. König, J. Schliemann, T. Jungwirth, and A. H. Mac Donald, cond-mat/0111314 (unpublished).
[4] S. C. Erwin and A. G. Pethukov, Phys. Rev. Lett. **89**, 227201 (2002).
[5] J. M. Sullivan and S. C. Erwin, Phys. Rev. B **67**, 144415 (2003).
[6] Y. D. Park, A. T. Hanbicki, S. C. Erwin, C. S. Hellberg, J. M. Sullivan, J. E. Mattson, T. F. Ambrose, A. Wilson, G. Spanos, and B. T. Jonker, Science **295**, 651 (2002).
[7] N. Pinto *et al.*, Phys. Status Solidi C **1**, 1748 (2004); J. Magn. Magn. Mater. **272**, 2006 (2004), and references therein.
[8] S. Cho, S. Choi, S. C. Hong, Y. Kim, J. B. Ketterson, B.-Jun Kim, Y. C. Kim, and J.-H. Jung, Phys. Rev. B **66**, 033303 (2002).
[9] S. Cho, S. Choi, S. C. Hong, Y. Kim, J. B. Ketterson, C.-U. Jung, K. Rhie, B.-J. Kim, and Y. C. Kim, Appl. Phys. Lett. **81**, 3606 (2002).
[10] S. Choi, S. C. Hong, S. Cho, Y. Kim, J. B. Ketterson, C.-U. Jung, K. Rhie, B.-J. Kim, and Y. C. Kim, J. Appl. Phys. **93**, 7670 (2003).
[11] G. Kioseoglou, A. T. Hanbicki, C. H. Li, S. C. Erwin, R. Goswami, and B. T. Jonker, Appl. Phys. Lett. **84**, 1725 (2004).
[12] Y. J. Zhao, T. Shishidou, and A. J. Freeman, Phys. Rev. Lett. **90**, 047204 (2003).
[13] E. Wimmer, H. Krakauer, M. Weinert, and A. J. Freeman, Phys. Rev. B **24**, 864 (1981); H. J. F. Jansen and A. J. Freeman, *ibid.* **30**, 561 (1984).
[14] A. Stroppa, S. Picozzi, A. Continenza, and A. J. Freeman, Phys. Rev. B **68**, 155203 (2003).
[15] A. J. R. da Silva, A. Fazzio, and A. Antonelli, cond-mat/0310770 (unpublished).
[16] M. Yu, C. S. Yavanthi, D. A. Drabold, and S. Y. Wu, Phys. Rev. B **64**, 165205 (2001).
[17] S. Baroni, A. Dal Corso, S. De Gironcoli, and P. Giannozzi, http://www.pwscf.org.
[18] A. Filippetti, N. Spaldin, and S. Sanvito, cond-mat/0302178 (unpublished).
[19] A. B. Shick, J. Kudrnovsky, and V. Drchal, Phys. Rev. B **69**, 125207 (2004).
[20] D. Vanderbilt, Phys. Rev. B **41**, 7892 (1990).
[21] H. J. Monkhorst and J. D. Pack, Phys. Rev. B **13**, 5188 (1976).
[22] N. J. Ramer and M. Rappe, J. Clin. Eng. **61**, 317 (2000).
[23] L. Kleinmann and D. M. Bylander, Phys. Rev. Lett. **48**, 1425 (1982).
[24] P. N. Keating, Phys. Rev. **145**, 637 (1966).
[25] Alex Zunger, S.-H. Wei, L. G. Ferreira, and James E. Bernard, Phys. Rev. Lett. **65**, 353 (1990).
[26] P. Boguslawski and A. Baldereschi, in *Proceedings of the 17th International Conference of the Physics of Semiconductors*, edited by J. D. Chadi and W. A. Harrison (Springer, New York, 1990), p. 939.
[27] A. Baldereschi and M. Peressi, J. Phys.: Condens. Matter **5**, B37 (1993).
[28] S. De Gironcoli, P. Giannozzi, and S. Baroni, Phys. Rev. Lett. **66**, 2116 (1991).
[29] J. C. Aubry, T. Tyliszczak, A. P. Hitchcock, J. M. Baribeau, and T. E. Jackman, Phys. Rev. B **59**, 180 (1999); P. Dismukes, L. Ekstrom, and R. J. Paff, J. Phys. Chem. **68**, 3021 (1964).
[30] F. Bernardini, S. Picozzi, and A. Continenza, Appl. Phys. Lett. **84**, 2289 (2004).
[31] P. O. Löwdin, J. Chem. Phys. **18**, 365 (1950).
[32] P. Mahadevan and A. Zunger, Phys. Rev. B **69**, 115211 (2004).
[33] M. Cococcioni and S. De Gironcoli, cond-mat/0405160 (unpublished).
[34] J. Okabayashi, A. Kimura, O. Rader, T. Mizokawa, A. Fujimori, T. Hayashi, and M. Tanaka, Phys. Rev. B **58**, R4211 (1998).
[35] J. Okabayashi, A. Kimura, T. Mizokawa, A. Fujimori, T. Hayashi, and M. Tanaka, Phys. Rev. B **59**, R2486 (1999).